

Soft Electronic Skin for Multi-Site Damage Detection and Localization

Eric J. Markvicka, Ravi Tutika, Michael D. Bartlett,* and Carmel Majidi*

Soft-matter technologies have a potentially central role in wearable computing, human–machine interaction, soft robotics, and other emerging applications that require highly compliant and elastic materials. However, these technologies are largely composed of soft materials that are susceptible to damage and loss of functionality when exposed to real-world loading conditions. To address this critical challenge, we present a soft responsive material that, like natural nervous tissue, is able to identify, compute, and signal damage in real-time. The soft composite material contains liquid metal droplets dispersed in an elastomer matrix that rupture when mechanical damage occurs (e.g., compression, fracture, or puncture), creating electrically conductive pathways. The resulting change in local conductivity can be actively sensed and coupled with actuation, communication, and computation in a manner that presents new opportunities to identify damage, calculate severity, and respond to prevent failure within soft material systems. When placed on the surface of a soft, humanoid-like inflatable structure, the skin can detect puncture damage and control the operation of an embedded fan to prevent deflation.

1. Introduction

Advances in soft-matter engineering have enabled the development of highly integrated, multifunctional materials capable of autonomous operation.^[1–3] Such materials have the potential to mimic the rich properties of skin, nervous tissue, and muscle for applications ranging from soft robotics,^[4–6] and “artificial skin” electronics for physiological monitoring and

human–machine interaction.^[7,8] As the performance and complexity of these systems continues to increase, uninterrupted monitoring of the integrity of individual soft material components becomes increasingly important. This requires the ability to track material and structural health through the detection of damage and propagation of flaws and defects. In more conventional material systems, damage has traditionally been detected through a variety of non-destructive evaluation (NDE) techniques, which can include ultrasonics, X-radiography, Eddy currents, magnetic techniques, and visual inspection.^[9,10] However, these systems are often bulky, can have strict material requirements (i.e., Eddy current approaches can only inspect conductive materials), and are more suited for periodic monitoring of damage in large-scale systems.^[11] Recent efforts have focused

on more scalable methods based on thin-film approaches that utilize visual inspection or ultrasonic techniques. Examples include the use of dye penetrants or mechanically induced color change through the use of specific chemical functional groups that undergo mechanochemical reactions.^[12–15] Despite their promise for certain monitoring conditions, these techniques often result in a limited visual signal and can require controlled lighting conditions to increase reliability.^[16] Micro-capsule techniques have recently demonstrated enhanced contrast with permanent color change.^[16] However, visual inspection is best suited for line of sight applications, can be tedious and time consuming, and potentially unreliable, which limits their use in autonomous and deployable systems.^[11] Compact piezoelectric or resistive systems can monitor damage remotely.^[17,18] However, these systems are typically composed of stiff (modulus > 1 GPa) and relatively brittle (strain < 10%) materials such as lead-zirconate-titanate (PZT) or polyvinylidene difluoride (PVDF), making them incompatible with soft and highly deformable materials and structures.^[19,20]

In the case of soft material systems, damage detection architectures must be mechanically compatible with the host structure. Human nervous tissue provides an example of a soft responsive material that is capable of detecting, communicating, and responding to harmful external stimuli (Figure 1a). The detection of adverse stimuli is initiated from an extensive network of cutaneous and subcutaneous receptors called nociceptors.^[21] The nociceptors are responsible for firing action potentials to directly relay this information to the cortex of the

Prof. E. J. Markvicka,^[†] Prof. C. Majidi
Soft Machines Lab
Carnegie Mellon University
Pittsburgh, PA 15213, USA
E-mail: cmajidi@andrew.cmu.edu
Prof. E. J. Markvicka, Prof. C. Majidi
Robotics Institute
Carnegie Mellon University
Pittsburgh, PA 15213, USA
R. Tutika, Prof. M. D. Bartlett
Materials Science & Engineering
Soft Materials and Structures Lab
Iowa State University
Ames, IA 50011, USA
E-mail: mbartlet@iastate.edu

 The ORCID identification number(s) for the author(s) of this article can be found under <https://doi.org/10.1002/adfm.201900160>.

^[†]Present address: Mechanical and Materials Engineering, University of Nebraska-Lincoln, Lincoln, NE 68588, USA

DOI: 10.1002/adfm.201900160

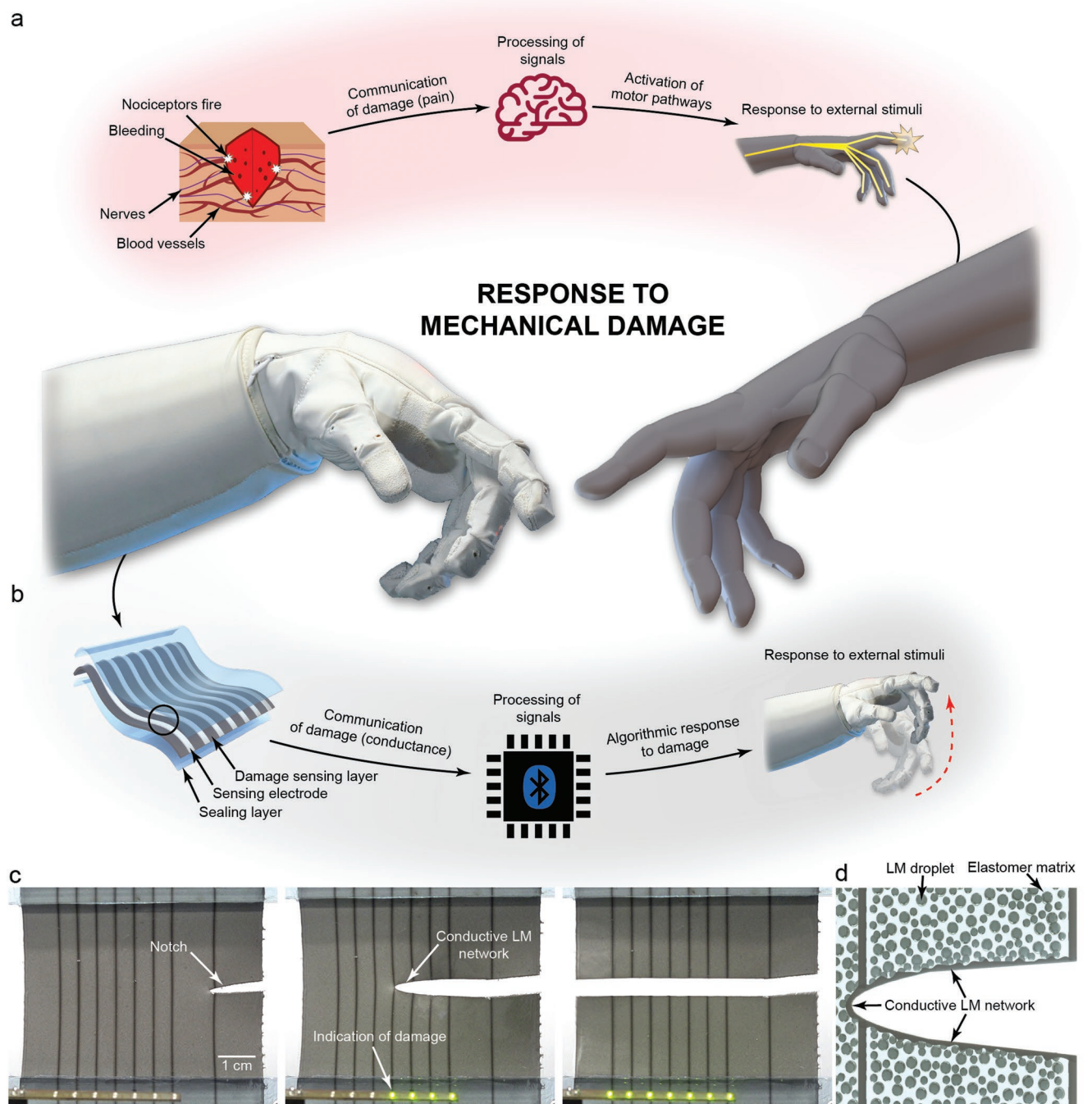


Figure 1. LM–elastomer composite for autonomous damage detection. a) Illustration of the human body’s response to harmful external stimuli: detection (firing of nociceptors), communication (firing of action potentials), and response (activation of motor pathways). b) Illustration of the artificial nervous tissue’s response to mechanical damage: detection (local change in conductivity), communication (flow of electrical current), and response (algorithmic response). c) Photograph sequence of a notched sample that is strained until mechanical failure. The propagation of the notch creates a conductive network, as indicated by the illumination of the green LEDs. d) The damage sensing composite is composed of microdroplets of LM embedded within a hyperelastic material that rupture upon induced mechanical damage, creating a percolating or continuous conductive network of LM.

brain. The human body responds by activating motor pathways to move the endangered appendage away from the external stimuli. This interconnected response in biological systems has inspired a wide range of stimuli-responsive materials that adapt

or respond to environmental changes including temperature, mechanical or physical, optical, and chemical.^[22–25] Bioinspired soft materials that exhibit similar response and which also interface with existing technologies provide a path forward to

enable intelligent, programmable interactions between external stimuli and dynamic material properties.^[1] Recently, autonomy has been incorporated in soft-matter systems through intelligent mechanical design with pre-planned tasks and on-board actuation, power, and computation.^[2,26–30] While promising, these systems lack the necessary hardware and sensing to provide critical run-time feedback to modify the pre-planned task. Additionally, for wireless machines in remote areas, power consumption needs to be minimized. This is critical for long-term remote monitoring of deployed systems to achieve system autonomy. The comprehensive system-level integration of components to enable soft-matter robotic materials to be fully self-aware of their current state still remains a significant challenge.

Here, we introduce a soft material architecture for “artificial nervous tissue,” that incorporates LM–elastomer composites and arrays of LM traces in a manner that enables active electrical detection and localization of multiple material damage events. The soft and elastically deformable “artificial nervous tissue” can detect and localize damage (Figure 1b) by monitoring the formation of conductive areas from damage related events such as compression, fracture, or puncture. When damage occurs, LM microdroplets within the LMEE will rupture and cause in situ conductive pathways between neighboring droplets to form, which is observed as a local change in electrical conductivity. To sense the local, discrete changes in electrical conductivity, a passive multiplexing technique is used, where a pair of electronic switches and a microcontroller is used to monitor the impedance between adjacent LM traces (Figure 1c) or at each node for overlapping arrays (Figure 4). By monitoring the formation, instead of destruction, of conductive networks, a large change in electrical signal is observed resulting in a nearly digital response to damage. Furthermore, the self-healing properties of the LM–elastomer composite allow the detection of multiple damage events along the same conductive LM trace in overlapping arrays. This ultimately provides a path forward for achieving the longevity that is exhibited in natural, biological systems. The electrical communication of damage enables direct integration with existing electronic control systems, providing a method for soft-matter robotic systems to initiate an algorithmic response to prevent failure. Due to the initially open circuit architecture (naturally, electrically insulating), the damage detection scheme requires ultra-low currents to monitor the undamaged state, as power is not dissipated across a resistive medium. To demonstrate the ability to detect, communicate, and respond to a potentially detrimental event, we integrate this material architecture with an untethered, inflatable soft humanoid structure, where multiple puncture events are rapidly detected, computed, and utilized in a control loop to prevent deflation and loss of functionality.

2. Results & Discussion

We realize this damage detecting material system using an LMEE material architecture, where Ga-based LM is shear mixed with uncured silicone elastomer at a 1:1 volume ratio, forming a suspension of LM microdroplets ($\approx 45 \mu\text{m}$ particles, Figures S1 and S2, Supporting Information).^[31] Previously, the authors and others have shown that LM-embedded elastomer

(LMEE) composites can be engineered to exhibit a wide range of material properties—including extreme toughening,^[32] exceptional electrical and thermal properties,^[33–40] and the ability to form electrically conductive pathways through controlled mechanical pressure^[31,41–44] or laser patterning^[45] that autonomously form new conductive pathways when the material is torn, punctured, or removed.^[31] Electrical conductivity is only possible with certain compositions and requires extreme pressure or stretch in order to rupture the embedded LM droplets and induce percolation. Electrical percolation is induced by large internal tensile stress concentrations that form around the LM inclusions.^[46] Upon application of sufficient pressure, the thin elastomer layer between inclusions ruptures, leading to the in situ flow of LM and formation of percolating electrical networks. While these previous efforts have examined the conductivity and electromechanical properties of LMEEs, the electrical response to damage is rarely studied and none of them have explored how load-controlled LM droplet percolation can be harnessed to detect and localize damage within a soft material system. Building upon this previous work, we tune the LMEE material architecture by varying the stiffness of the elastomer matrix and examine its influence on the response of LMEEs to mechanical loading and damage. Electrical conductivity is observed to generally increase with volume loading of LM (Figure S3, Supporting Information). For this study, we concentrate on the composite with the highest electrical conductivity ($\phi = 50\%$). In particular, we show that LMEEs can be incorporated into a soft materials architecture that electrically registers the occurrence and location of mechanical damage caused by compression, fracture, or puncture (Figure 1c,d). When damaged, LM microdroplets within the LMEE will rupture and cause in situ conductive pathways between neighboring droplets to form (Figure 1d). The damage-initiated change in electrical conductivity enables mechanical damage to be actively detected and localized, as indicated by the illumination of the LEDs as a notch propagates through the specimen (Figure 1c and Video S1, Supporting Information). The fracture process zone experiences high local strains that result in the formation of an internal percolating network and local change in the electrical conductivity. Because this process zone extends beyond the immediate boundaries of a tear, we observe that the LEDs are illuminated before the notch reaches the conductive trace. Additionally, the internal LM percolation associated with this response can be coupled with optical cues that are analogous to skin bruising (Figure S4, Supporting Information). Compared to other multi-point methods such as electrical impedance tomography that monitor the loss in conductivity,^[47–49] or increase in resistance, across a film, the damage detection scheme presented here requires lower currents to monitor the undamaged state, due to the initially open circuit architecture (naturally, electrically insulating).

2.1. Mechanical Characterization

The damage sensing layer is composed of Ga-based LM that is shear mixed with uncured silicone elastomer at a 1:1 volume ratio, forming a suspension of LM microdroplets ($\approx 45 \mu\text{m}$ particles, Figures S1 and S2, Supporting Information).^[31]

This architecture provides significant stress shielding from unintended activation over other droplet film type architectures.^[42] We utilize an elastomer blend of Sylgard 184 and Sylgard 527^[50] to tailor the mechanical characteristics of the solid–liquid hybrid composite and its sensitivity to mechanical damage. The mechanical behavior of the LM–elastomer composite ($\phi = 50\%$) is studied under tensile loading for two oligomer/curing agent ratios (5:1, 10:1; $\alpha = 100\%$) and four different blends of Sylgard 184 and Sylgard 527 ($\alpha = 80, 60, 40, 20\%$, where α is the ratio of Sylgard 184 to Sylgard 527). Figure 2a presents the stress–strain curves for the different LM–elastomer composites. From this data, the influence of the liquid inclusions is studied by measuring the tensile modulus of the filled, E_c , and unfilled, E_e , elastomer. Figure 2b shows that the LM inclusions soften the compliant-matrix. These results generally agree with Eshelby's inclusion theory,^[51] $E_c = E_e/(1 + 5\phi/3)$, assuming incompressible fluidic inclusions ($E_i = 0$ Pa). Referring to Figure 2b (inset), both the experimental results and theory suggest an approximately 50% decrease in the stiffness with the addition of LM inclusions ($\phi = 50\%$). As shown in Figure 2c, the elastic strain limit of the elastomer and composite generally increases with increasing compliance. While, the LM inclusions have a negligible influence on the strain limit of the elastomer composite, they can significantly

increase the toughness of the host elastomer by resisting fracture propagation.^[32] Furthermore, when used as a coating, the LM composite has a negligible influence on the stress–strain response of Nylon fabric (Figure 2d). Here, we observe that LM inclusions increase the compliance of the soft, silicone rubber, while maintaining the elastic strain limit. This desirable combination of properties is uniquely enabled by the inclusion of liquid metal droplets, which preserve the properties of the host material and enable electronic damage detection and localization.

2.2. Formation of Electrical Networks

The LM–elastomer composite is (naturally) electrically insulating after curing due to the presence of an insulating oxide skin on the surface of the LM droplets and lack of droplet–droplet contact (or percolating networks). However, the application of local pressure or various modes of mechanical damage (e.g., cutting, puncture, large strain deformation) can cause the LM inclusions to rupture, forming a conductive percolating network (conductance between two adjacent traces, $G > 0.003$ S) that is internal to the composite with a minimum thickness of 200 μm (Figure S5 and Table S1,

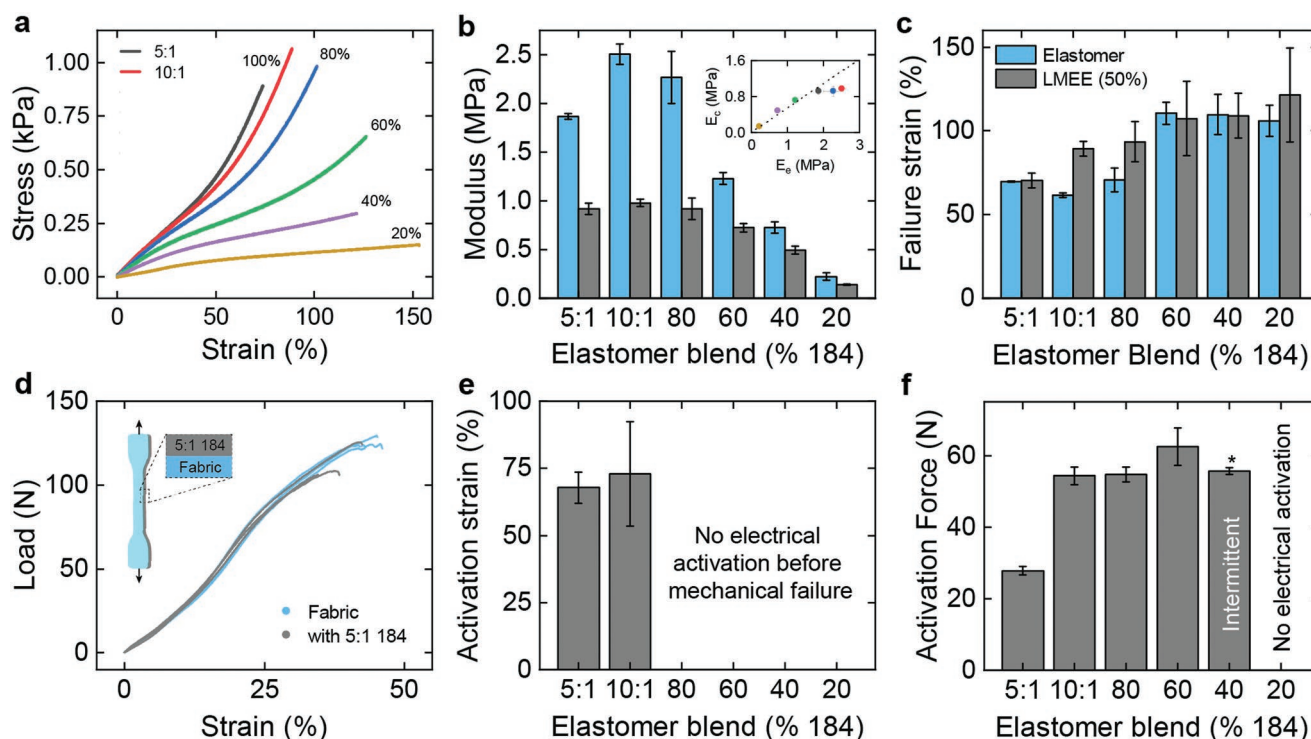


Figure 2. Mechanical and electrical characterization. a) Stress–strain response under uniaxial extension to mechanical failure for two oligomer/curing agent ratios (5:1, 10:1; $\alpha = 100\%$) and four different blends of Sylgard 184 and Sylgard 527 ($\alpha = 80, 60, 40, 20\%$, where α is the ratio of Sylgard 184 to Sylgard 527). b) Modulus as a function of elastomer blend ($\phi = 0, 50\%$). Inset: Composite modulus, E_c , as a function of elastomer modulus, E_e , and Eshelby's inclusion theory (dashed line), assuming incompressible fluidic inclusions, $E_i = 0$ Pa. c) Mechanical failure strain as a function of elastomer blend ($\phi = 0, 50\%$). d) There is a negligible influence on the stress–strain response of ripstop nylon fabric when coated with the LM–elastomer composite. All error bars are the standard deviation. e) Uniaxial extension strain upon which an electrical network is formed. For samples blended with Sylgard 527, an electrical network did not form before mechanical failure. f) Compression force required to cause the formation of an electrical network. Electrical activation was intermittent for the $\alpha = 40\%$ blend and did not occur for approximately half of the samples tested ($N = 12$). (b)–(d) $N = 3$, (e) $N = 5$.

Supporting Information). The damage-initiated change in electrical conductivity was systematically studied for the different elastomer blends and various modes of mechanical damage. First, the electrical conductivity was monitored between two conductive tabs of a dogbone specimen under uniaxial deformation. As shown in Figure 2e, only the Sylgard 184 specimens ($\alpha = 100\%$) formed an electrical network before mechanical failure occurred. The composite was then subjected to mechanical compression. A glass cylindrical indenter (3 mm diameter, 10 mm length) was pressed into the composite across two conductive traces until an electrical network was formed. As shown in Figure 2f, without puncture, a large compressive force is required to form an internal, percolating electrical network. The softer LM–elastomer composites either did not form an electrical network under compression ($\alpha = 20\%$) or only achieved intermittent activation (6 of 12, $\alpha = 40\%$) that was typically not permanent (Figure S6, Supporting Information). To differentiate between compression and puncture, the $\alpha = 20\%$ composite could be combined with a $\alpha \geq 60\%$ composite. If puncture occurs, both composites would be activated. If concentrated compression occurs, only the $\alpha \geq 60\%$ composite would be activated. Lastly, all elastomer blend composites were observed to form an electrical network when cut with a precision knife. **Figure 3a** shows the formation of a permanent electrical network as indicated by the illumination of the

green LEDs as the knife passes through the material. During puncture events, such as cutting, the LM droplets on the damaged surface are severed in addition to the formation of an internal percolating network (Figure 3a, inset). In the presence of oxygen, an oxide skin is formed on the exposed LM, preventing unwanted flow of LM. These results demonstrate that the composite is stable under typical operational conditions and that the mechanical properties of the composite can be easily tuned without increasing the overall thickness of the device to achieve damage-initiated conductivity only when puncture occurs.

2.3. Integrating with Host Substrates

To demonstrate the ability to integrate the active damage layer with existing structures, the composite was coated on a variety of commonly used materials including fabric (nylon, polyester), plastic (polyethylene terephthalate (PET), acrylonitrile butadiene styrene (ABS)), and metal (aluminum). As shown in Figure 3b, the composite can be directly coated and cured on a variety of materials or attached using a silicone glue (Silpoxy, Smooth-On). When coated on flexible substrates (fabric, thin plastic film), the soft and highly compliant LM–elastomer composite is electrically stable and does not restrict the general kinematic motion of the flexible substrate (Figure 3b).

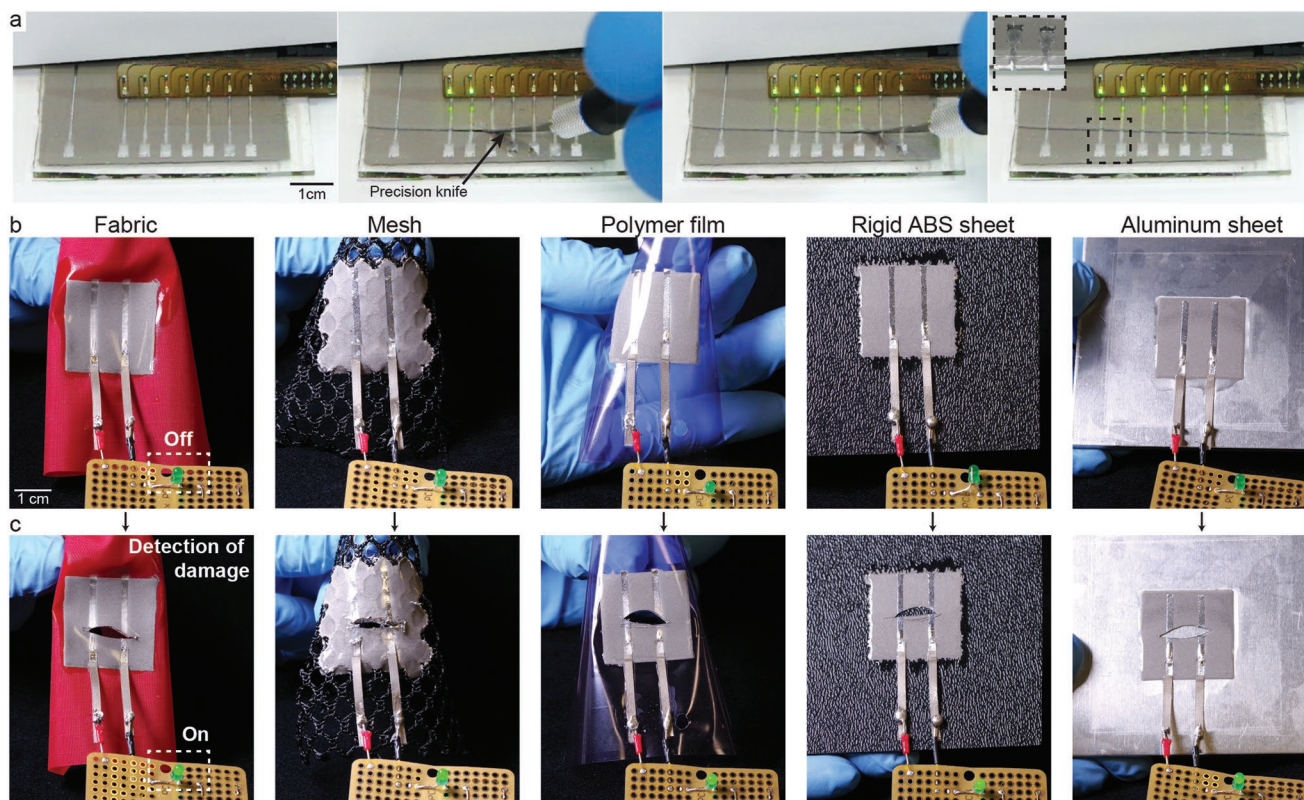


Figure 3. Damage detection substrate versatility. a) Photograph sequence of mechanical damage induced by a precision knife. The propagation of damage is indicated by the green LEDs. Inset: photograph of the cut surface. b) The damage sensing composite is then fabricated on a variety of substrates while maintaining electrical insulation. c) Upon cutting the substrate, the material activates on all substrates (bottom row), as indicated by the illuminated LED.

Additionally, as a coating, the LM–elastomer composite is able to detect damage as indicated by the illuminated LED (Figure 3c)—similar to what was shown in Figure 1 for the free-standing elastomer. These results demonstrate that the composite can be used as a coating to detect damage on a variety of substrates, ranging from flexible to rigid, polymeric to metallic, and porous to continuous.

2.4. Detection and Localization of Damage

The LM–elastomer composite reports changes in structural or material health by detecting local changes in electrical conductivity. To sense the local, discrete changes, a passive multiplexing technique is used to monitor the impedance between adjacent LM traces in 1D samples (Figure 1c) or at

each node, or crossing, of the overlapping arrays in 2D samples (Figure 4). The highly deformable liquid metal traces are spray deposited^[52] onto the LMEE composite (sensing layer) and sealed in a thin elastomer layer ($t = 0.5$ mm) to prevent smearing. For 2D detection and localization, a second array is spray deposited on the opposite side, forming a 10×10 active-matrix grid to monitor through-thickness conductivity (Figure 4a). A pair of electronic switches and a microcontroller with an analog to digital converter (ATmega 328, Atmel) is used to monitor the impedance at each of the nodes, or crossings, within the grid (Figure 4b). First, as illustrated in Figure 4c, the demultiplexing switch applies a voltage potential to an individual trace (blue traces). The multiplexing switch then scans all the orthogonal traces (red traces). If a voltage is sensed on an orthogonal trace, damage has occurred at the intersection of the two traces, as illustrated in Figure 4c. The demultiplexing

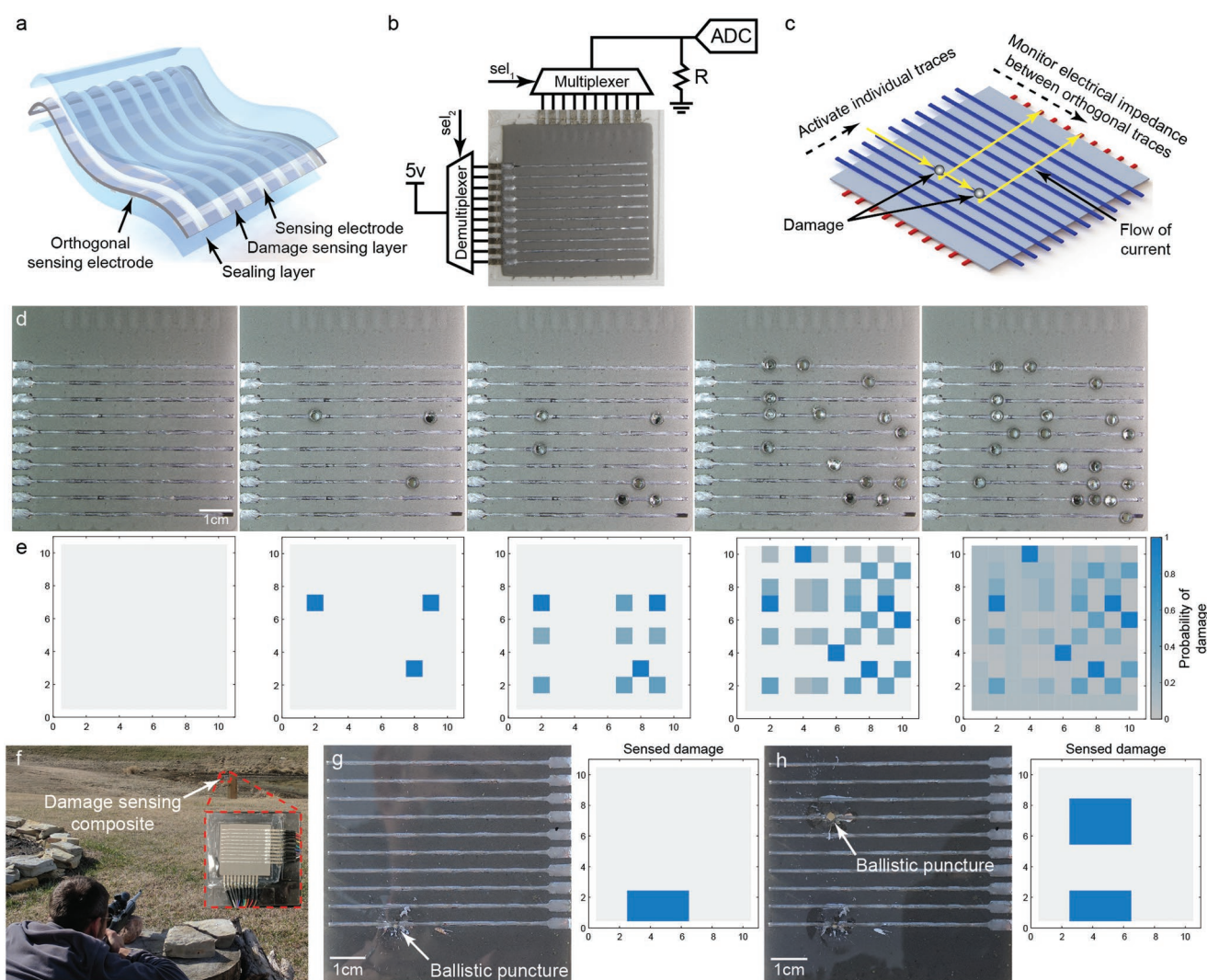


Figure 4. Damage detection and 2D localization. a) Illustration of the damage detection composite with spray deposited 2D grid of LM. b) Electrical circuit used to detect and localize changes in conductivity (damage). c) Current flows through the thickness of the composite when mechanical damage occurs. d) A random sequence of 19 damage events and e) the estimated probability of damage. The hue of each node is proportional to the probability of damage at that location. f) Two projectiles were fired at the damage sensing composite using a .22-caliber long rifle. g, h) (left) The projectile passed through the composite that was supported as a membrane on an acrylic frame; (right) damage was detected and localized as indicated by the blue nodes.

switch is then indexed to the next trace and the orthogonal traces are scanned again.

To demonstrate this method for detecting and localizing damage, a hammer-driven hole punch (3 mm diameter) was used to induce mechanical damage at a sequence of specified nodes. The electrically self-healing properties of the LM–elastomer composites enable multiple damage events along the same conductive LM trace, even when portions of the LM trace are completely removed. During damage, the LM traces are electrically connected to the LMEE composite allowing the severed trace to be automatically reconfigured around the damage region without the loss of conductivity. With this sensing scheme and material architecture, the first two damage events will always be detected with 100% probability and is observed as the minimum number of fully localized damage locations (100% probability) for any active-matrix grid that is at least 2×2 in size (Figure S7b, Supporting Information). In contrast, for the extreme (and rare) case when damage localizes along one vertical line and one horizontal line, the same 10×10 (M rows \times N columns) active-matrix grid can detect and localize up to 18 locations, or $M+N-2$, with 100% probability (Figure S7d, Supporting Information). For both cases, there are $M+N-1$ independent events, that is, changes in state, where a new damage event is detected and localized.

Figure 4d shows a random sequence of damage events that resulted in six locations of 100% probability along with many more locations where damage is uncertain. The calculated probability of damage is plotted in Figure 4e, where the hue of each of the nodes is proportional to the probability of damage at that location. As observed after six damage events (Figure 4d,e, center), there are four locations where no damage has occurred: (2,2), (7,7), (7,5), and (9,5). This phantom damage signal occurs when multiple locations are activated after a single damage event. To account for this uncertainty, the probability of damage was calculated as $1/(\text{number of activated nodes})$. For example, when damage occurs at location (9,2), two new locations are detected (9,2) and (2,2), resulting in a 50% probability of damage at each location (see Figure S8, Supporting Information for additional details). The goal of this damage sensing scheme and material architecture is not to localize every damage event with absolute certainty, since a large number of damage events would likely lead to an irrecoverable state. Instead, the purpose is to introduce an artificial nervous tissue that extends the longevity of soft-matter systems by reporting initial occurrences of damage with high probability, while determining severity to allow the host system to respond. To improve accuracy over a large area, multiple active-matrix arrays could be combined on the same surface or object. These experiments highlight the composite's unique ability to detect and localize multiple extreme damage events with high probability, without experiencing catastrophic failure when the active-matrix grid is severed or portions are completely removed.

3. Demonstrations

The previous subsections report on material responses within a controlled laboratory setting. To further examine the effects

of extreme damage in an uncontrolled environment, the 2D composite was subjected to ballistic puncture in an outdoor firing range. The composite was suspended as a membrane on an acrylic frame and two projectiles were fired from a .22-caliber long rifle (10/22, Ruger) at a distance of approximately 25 meters (Figure 4f). The projectile impact resulted in a fairly large damage zone that is instantaneously activated (Figure 4g,h, left). The projectile exit is shown in Figure S9, Supporting Information. The detected damage zone is significantly larger than the entrance or exit hole due to the ballistic shock wave that is generated by the bullets (Figure 4g,h, right). Although limited to a single demonstration, these results nonetheless show the composite's ability to detect and localize extreme damage in a real-world setting.

The electrical response to damage enables integration with existing control systems and provides unique opportunities to monitor structural health within soft robots or inflatable structures. Here, we use the composite to augment the exterior of an inflatable, untethered soft structure intended to mimic a soft humanoid robot (Figure 5a). The soft robot mimic is composed of a fabric suit, a fan that continuously runs to compensate for leaks, a high-resolution, absolute barometric pressure sensor (BMP280, Bosch), and a plastic skeleton to support the suit (Figure S10, Supporting Information). The fan is set to the minimum velocity required to maintain sufficient inflation, as shown in Figure 5c,d (left). Three holes, approximately 625 mm^2 in size, are cut into the soft robot mimic with a precision knife. In the absence of damage detection and closed-loop control, the soft robot mimic quickly deflates as the hole size increases (Figure 5c, left to right). The internal pressure of the inflatable structure was continuously monitored using an absolute barometric pressure sensor (Figure 5e, red, bottom). The damage events are clearly distinguishable and appear as sharp decreases in the monitored pressure due to the rapid flow of air leaving the puncture site. However, while an overall decrease in pressure was expected, the monitored change in pressure from the original to final state is on the order of the noise of the high-resolution pressure sensor ($\Delta P < 10 \text{ Pa}$). Consequently, it would be difficult to use this type of transducer for closed-loop control of low-pressure, inflatable structures. In contrast, the soft robot mimic that is augmented with the damage sensing composite is capable of detecting and responding to the external damage (Figure 5d). After detection by the microcontroller, the damage signals are wirelessly transmitted to a mobile computing platform and the effective area of damage is calculated (Figure 5e, top). Based on the calculated damage, the on-board control system is able to adjust the velocity of the fan used for inflation to compensate for the loss in pressure caused by the damage (Figure 5d, inset). Here, a small increase in pressure is observed as damage is induced (Figure 5e, gray, bottom). The relative progression of damage is also shown in Video S2, Supporting Information. This demonstration illustrates the ease of integration with existing soft-matter systems and compatibility with on-board control, sensing, and actuation commonly used in existing robotic platforms. As with the ballistic impact study, it also provides evidence that the damage-detecting material can function outside of a controlled laboratory setting.

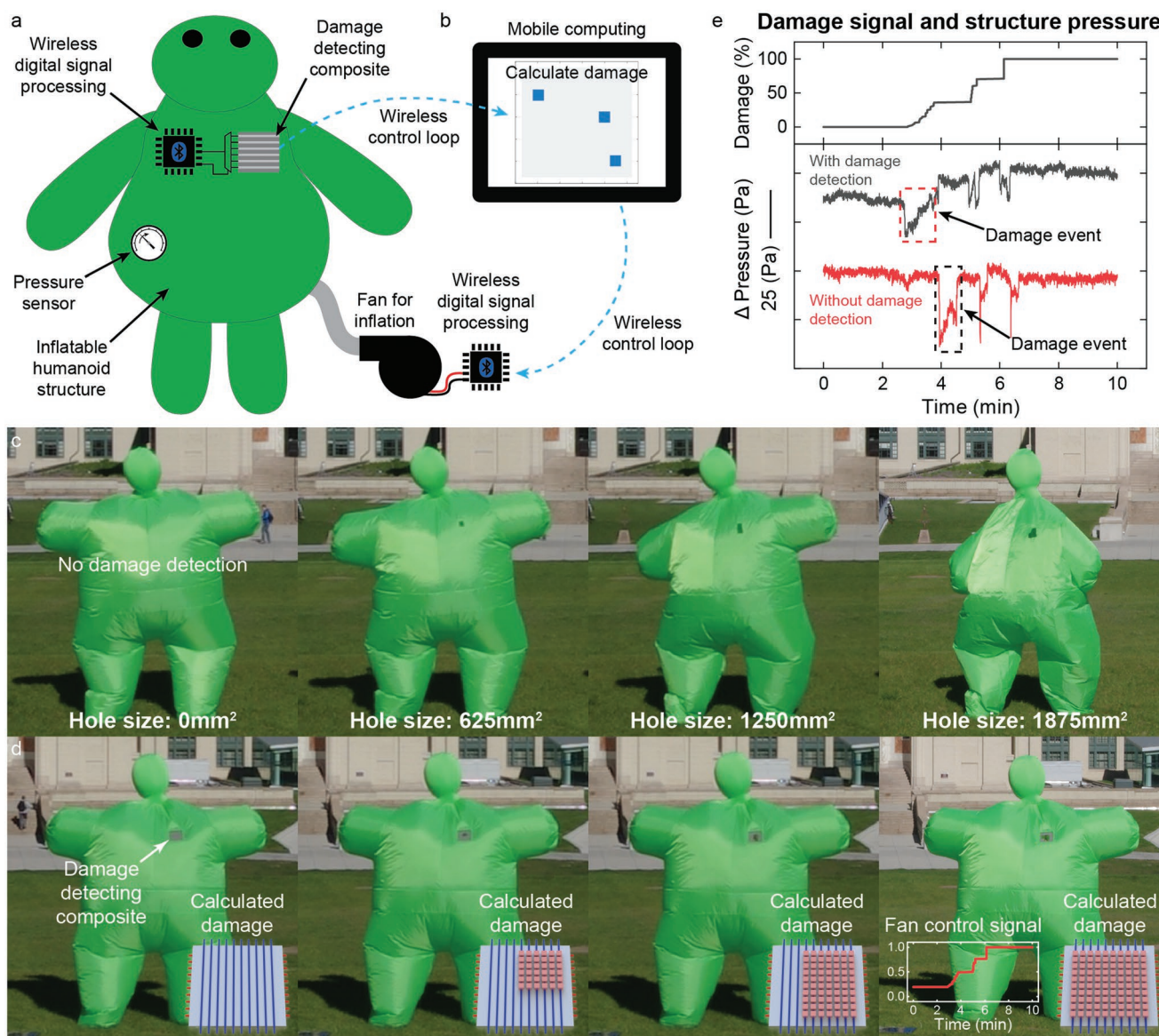


Figure 5. Autonomous damage detection for pressure regulation. a) A soft, untethered inflatable humanoid structure with programmable fan for inflation was augmented with the damage detecting composite. The fan is shown outside of the inflatable structure for visualization. b) A mobile computing platform is used for visualization of damage, recording damage and pressure data, and provides a wireless link between the damage detecting composite and programmable fan. c,d) Damage was induced using a precision knife. (c) The unmodified inflatable humanoid structure was unable to detect any environmental changes and quickly deflated as the area of damage increased. (d) The augmented inflatable humanoid structure was able to detect and respond to the environmental changes by increasing the velocity of the fan based on the estimated area of damage. (inset) Plot of the fan control signal. When damage is detected, the velocity of the fan is increased to compensate for the loss in pressure. (c) (bottom) Approximate area of damage. (e) (top) Plot of the estimated damage. (e) (bottom) The change in pressure (red) of the inflatable humanoid structure is almost undetectable using a high resolution barometer (± 1 Pa). In contrast, the pressure (gray) of the augmented inflatable structure slightly increases as damage occurs. e) Note, a y axis offset is applied to the data to assist in visualization of the data.

4. Conclusion

We have presented a soft biomimetic composite for use as artificial nervous tissue to detect, communicate, and respond to detrimental, mechanical damage events. Mechanical damage—that is, compression, fracture, or puncture—causes embedded droplets of liquid metal (LM) suspended in a soft elastomer matrix to rupture, creating local changes in electrical conductivity. This work builds off of previous studies by the authors

on damage-induced percolation of LM droplets within LM-embedded elastomer (LMEE) composites. What is new here is the special focus on how the mechanical compliance of the elastomer matrix can be used to tailor the damage response of LMEEs such that changes in electrical conductivity only occur for certain types of damage. Another novel contribution is the integration of a highly deformable active-matrix grid of LM traces that measure these local changes in conductivity in order to actively detect and localize the material damage.

Furthermore, we show such a composite can be coated on a variety of substrates and is observed to operate as expected even under extreme damage events such as ballistic puncture. When tightly coupled with actuation, computation, and communication, this system provides a method for structural health monitoring in an inflatable soft robot mimic, enabling algorithmic adaptation to environmental changes. This technology, coupled with methods for self-healing, provides a path forward for continuous structural health monitoring, self-diagnosis, and repair of soft structures to rival the longevity that is exhibited in natural, biological systems.

5. Experimental Section

Fabrication: Sylgard 184 (Dow Corning) was prepared per manufacturer's directions by mixing 10:1 oligomer-to-curing agent ratio in a planetary centrifugal mixer, unless otherwise noted. The Sylgard 184 5:1 specimens were prepared by mixing 5:1 oligomer-to-curing agent ratio. Sylgard 527 (Dow Corning) was prepared per manufacturer's directions by mixing equal weights of parts A and B in a planetary centrifugal mixer. The elastomer blends were prepared by mixing 80%, 60%, 40%, and 20% weight percent of Sylgard 184 to Sylgard 527 in a planetary centrifugal mixer. All base elastomers (Sylgard 184 and 527) were mixed for 1 min and then defoamed for 1 min using a planetary mixer (AR-100, Thinky). Gallium and indium were purchased from Solution Materials, LLC and combined at 75% Ga, 25% In by weight to produce EGaln. The LM–elastomer composite was fabricated by combining uncured silicone with EGaln at a 1:1 volume loading. The prepolymer and LM were mixed by hand until an emulsion was formed and no large droplets of LM were visually present. The emulsion was then further mixed using a planetary mixer for 1 min (AR-100, Thinky). After mixing, the composite was cast or molded and subsequently cured (100 °C, 1 h).

Mechanical Characterization: Samples were cast in acrylic molds ($t = 1$ mm) using a dogbone specimen geometry (Die B, ASTM D412A) and tested on a materials testing machine (5969, Instron) at a strain rate of 100 mm·min⁻¹. To prevent slipping, the samples were glued (Sil-Poxy, Smooth-On) to 6 mm thick acrylic plates and allowed to cure overnight. The LM–elastomer composite was coated on ripstop Nylon (xprd560961, Jo-Ann Fabrics). A dogbone specimen geometry was cut from the sheet using a UV laser cutter (U3 protolaser, LPKF).

Electrical Characterization: Activation strain: Samples were cast in acrylic molds ($t = 1$ mm) using a dogbone specimen geometry (Die B, ASTM D412A) and tested on a materials testing machine (5969, Instron) at a strain rate of 100 mm·min⁻¹. The tabs of the specimen were activated to the gauge by manually applying pressure. The samples were then glued (Sil-Poxy, Smooth-On) to 6 mm thick acrylic plates and allowed to cure overnight, with the electrical contact outside of the clamping area to reduce possible artifacts. The conductivity between the tabs was monitored using a Universal Serial Bus (USB) DAQ (USB-6002, NI). In its undamaged state following synthesis, this composite was electrically insulating ($<10^{-7}$ S), even for high liquid metal volume fractions ($\phi \geq 50\%$). Once activated, the conductivity for a $\phi = 50\%$ composite was $\sigma = 1.37 \times 10^3$ S·cm⁻¹. During characterization, we considered the composite to be fully activated when the conductance between two adjacent traces was $G > 0.003$ S.

Activation Force: The LM–elastomer composite was cast in square acrylic molds ($t = 500$ μm). Traces were drawn into the material using a ball point pen with a center-to-center spacing of 5 mm. The samples were then encapsulated with a 500 μm layer of 10:1 Sylgard 184 (cured at 100 °C for 30 min). A glass cylindrical indenter (3 mm diameter) was pressed into the composite at a rate of 0.01 mm·s⁻¹. For cut activation, a precision knife was used to cut across two adjacent traces. The conductivity between adjacent lines was monitored using a USB DAQ (USB-6002, NI).

Active-Matrix Grid of LM: For 1D samples, a grid of LM was spray deposited^[S2] onto the LM–elastomer composite using a stencil mask (Blazer Orange Laser Mask, IKONICS Imaging). Conductive fabric tape (CN-3490, 3M) was used to interface the LM traces with hook up wiring. The circuit schematic for 1D damage detection is shown in Figure S11, Supporting Information.

For 2D samples, a grid of LM was spray deposited^[S2] onto an elastomer sealing layer using a stencil mask (Blazer Orange Laser Mask, IKONICS Imaging). The LM–elastomer layer was deposited on top of the grid using a thin-film applicator (ZUA 2000, Zehntner) and cured (100 °C, 1 h). A grid of LM was then spray deposited^[S2] onto the LM–elastomer composite. Conductive fabric tape (CN-3490, 3M) was used to interface the LM traces with hook up wiring. For detecting and localizing damage, an electronic switch (CD74HC4067SM96, TI) was used in a multiplexer/demultiplexer configuration as shown in Figure 4b. A microcontroller (ATMega 328) was used to interface with a computer using the USB. The data was plotted using server-side JavaScript (Node.js).

Soft Robot Fabrication: The soft robot mimic was constructed from a fabric suit (inflatable full body suit, Rubie's), two squirrel cage fans (11270, SparkFun Electronics) that continuously ran to compensate for leaks within the fabric suit, and a PVC skeleton to support the fabric suit (Figure S10, Supporting Information). A Bluetooth low energy (BLE) UART module (nRF51, Nordic) was connected to the microcontroller, enabling wireless data transmission to a mobile computing platform (Pixel C, Google). The estimated damage was calculated and sent to a second microcontroller (ATMega 328) with a BLE UART module. A DC motor driver (DRV8871, TI) was used to control the velocity of the fans used for inflation. The circuit was powered using two lithium ion batteries (3.7v, 2000 mAh) connected in series. The internal structure pressure was monitored using a high resolution, absolute barometric pressure sensor (BMP280, Bosch).

Supporting Information

Supporting Information is available from the Wiley Online Library or from the author.

Acknowledgements

The authors acknowledge support from the NASA Early Career Faculty Award (NNX14AO49G; Research Collaborator: Dr. Bill Bluethmann), AFOSR Multidisciplinary University Research Initiative (FA9550-18-1-0566; Program Manager: Dr. Ken Goretta), Army Research Office (W911NF-18-1-0150; Program Manager: Dr. Sam Stanton), and Iowa State University through start up funds. Sensor and mechanical characterization was performed on equipment supported through an Office of Naval Research (ONR) Defense University Research Instrumentation Program (DURIP) (N00014140778; Bioinspired Autonomous Systems; PM: Dr. Tom McKenna).

Conflict of Interest

The authors declare no conflict of interest.

Keywords

damage detection, electronic skins, liquid metals, robotics, stretchable electronics

Received: January 5, 2019

Revised: May 4, 2019

Published online:

- [1] M. A. McEvoy, N. Correll, *Science* **2015**, *347*, 1261689.
- [2] M. Wehner, R. L. Truby, D. J. Fitzgerald, B. Mosadegh, G. M. Whitesides, J. A. Lewis, R. J. Wood, *Nature* **2016**, *536*, 451.
- [3] P. M. Reis, H. M. Jaeger, M. van Hecke, *Extreme Mech. Lett.* **2015**, *5*, 25.
- [4] C. Laschi, B. Mazzolai, M. Cianchetti, *Sci. Robot.* **2016**, *1*, eaah3690.
- [5] S. I. Rich, R. J. Wood, C. Majidi, *Nat. Electron.* **2018**, *1*, 102.
- [6] J. Wu, S.-Y. Tang, T. Fang, W. Li, X. Li, S. Zhang, *Adv. Mater.* **2018**, *30*, e1805039.
- [7] M. L. Hammock, A. Chortos, B. C.-K. Tee, J. B.-H. Tok, Z. Bao, *Adv. Mater.* **2013**, *25*, 5997.
- [8] T. Q. Trung, N.-E. Lee, *Adv. Mater.* **2016**, *28*, 4338.
- [9] L. Cartz, *Nondestructive Testing*, ASM International **1995**.
- [10] O. Salawu, *Eng. Struct.* **1997**, *19*, 718.
- [11] K. K. Tseng, L. Wang, *Smart Mater. Struct.* **2004**, *13*, 1017.
- [12] J. Pang, I. Bond, *Compos., Part A* **2005**, *36*, 183.
- [13] D. A. Davis, A. Hamilton, J. Yang, L. D. Cremer, D. Van Gough, S. L. Potisek, M. T. Ong, P. V. Braun, T. J. Martínez, S. R. White, J. S. Moore, N. R. Sottos, *Nature* **2009**, *459*, 68.
- [14] J. F. Patrick, M. J. Robb, N. R. Sottos, J. S. Moore, S. R. White, *Nature* **2016**, *540*, 363.
- [15] O. Rifaie-Graham, E. A. Apebende, L. K. Bast, N. Bruns, *Adv. Mater.* **2018**, *30*, 1705483.
- [16] W. Li, C. C. Matthews, K. Yang, M. T. Odarczenko, S. R. White, N. R. Sottos, *Adv. Mater.* **2016**, *28*, 2189.
- [17] F. N. Meyers, K. J. Loh, J. S. Dodds, A. Baltazar, *Nanotechnology* **2013**, *24*, 185501.
- [18] D. Ryu, K. J. Loh, *Smart Mater. Struct.* **2012**, *21*, 065016.
- [19] S. S. Kessler, S. M. Spearing, C. Soutis, *Smart Mater. Struct.* **2002**, *11*, 269.
- [20] R. Monkhouse, P. Wilcox, P. Cawley, *Ultrasonics* **1997**, *35*, 489.
- [21] D. Purves, G. Augustine, D. Fitzpatrick, L. Katz, A. LaMantia, J. McNamara, S. Williams, *Neuroscience*, Sinauer Associates, Sunderland, MA **2001**.
- [22] M. A. C. Stuart, W. T. Huck, J. Genzer, M. Müller, C. Ober, M. Stamm, G. B. Sukhorukov, I. Szleifer, V. V. Tsukruk, M. Urban, F. Winnik, S. Zauscher, I. Luzinov, S. Minko, *Nat. Mater.* **2010**, *9*, 101.
- [23] D. Roy, J. N. Cambre, B. S. Sumerlin, *Prog. Polym. Sci.* **2010**, *35*, 278.
- [24] P. Theato, B. S. Sumerlin, R. K. O'Reilly, T. H. EppsIII, *Chem. Soc. Rev.* **2013**, *42*, 7055.
- [25] Y. Kim, A. Chortos, W. Xu, Y. Liu, J. Y. Oh, D. Son, J. Kang, A. M. Foudeh, C. Zhu, Y. Lee, S. Niu, J. Liu, R. Pfattner, Z. Bao, T. W. Lee, *Science* **2018**, *360*, 998.
- [26] S. Felton, M. Tolley, E. Demaine, D. Rus, R. Wood, *Science* **2014**, *345*, 644.
- [27] C. D. Onal, D. Rus, *Bioinspir. Biomim.* **2013**, *8*, 026003.
- [28] A. D. Marchese, C. D. Onal, D. Rus, *Soft Rob.* **2014**, *1*, 75.
- [29] N. W. Bartlett, M. T. Tolley, J. T. Overvelde, J. C. Weaver, B. Mosadegh, K. Bertoldi, G. M. Whitesides, R. J. Wood, *Science* **2015**, *349*, 161.
- [30] P. Rothemund, A. Ainla, L. Belding, D. J. Preston, S. Kurihara, Z. Suo, G. M. Whitesides, *Sci. Rob.* **2018**, *3*, eaar7986.
- [31] E. J. Markvicka, M. D. Bartlett, X. Huang, C. Majidi, *Nat. Mater.* **2018**, *17*, 618.
- [32] N. Kazem, M. D. Bartlett, C. Majidi, *Adv. Mater.* **2018**, *30*, e1706594.
- [33] S. H. Jeong, S. Chen, J. Huo, E. K. Gamstedt, J. Liu, S.-L. Zhang, Z.-B. Zhang, K. Hjort, Z. Wu, *Sci. Rep.* **2015**, *5*, 18257.
- [34] E. Palleau, S. Reece, S. C. Desai, M. E. Smith, M. D. Dickey, *Adv. Mater.* **2013**, *25*, 1589.
- [35] G. Li, X. Wu, D.-W. Lee, *Lab Chip* **2016**, *16*, 1366.
- [36] M. D. Bartlett, A. Fassler, N. Kazem, E. J. Markvicka, P. Mandal, C. Majidi, *Adv. Mater.* **2016**, *28*, 3726.
- [37] M. D. Bartlett, N. Kazem, M. J. Powell-Palm, X. Huang, W. Sun, J. A. Malen, C. Majidi, *Proc. Natl Acad Sci. U.S.A.* **2017**, *114*, 201616377.
- [38] R. Tutika, S. H. Zhou, R. E. Napolitano, M. D. Bartlett, *Adv. Funct. Mater.* **2018**, *28*, 1804336.
- [39] M. I. Ralphs, N. Kemme, P. B. Vartak, E. Joseph, S. Tipnis, S. Turnage, K. N. Solanki, R. Y. Wang, K. Rykaczewski, *ACS Appl. Mater. Interfaces* **2018**, *10*, 2083.
- [40] A. Koh, J. Sietins, G. Slippher, R. Mrozek, *J. Mater. Res.* **2018**, *33*, 1.
- [41] J. W. Boley, E. L. White, R. K. Kramer, *Adv. Mater.* **2015**, *27*, 2355.
- [42] M. G. Mohammed, R. Kramer, *Adv. Mater.* **2017**, *29*, 19.
- [43] Y. Lin, C. Cooper, M. Wang, J. J. Adams, J. Genzer, M. D. Dickey, *Small* **2015**, *11*, 6397.
- [44] A. Fassler, C. Majidi, *Adv. Mater.* **2015**, *27*, 1928.
- [45] S. Liu, M. Yuen, E. L. White, J. W. Boley, B. Deng, G. J. Cheng, R. Kramer-Bottiglio, *ACS Appl. Mater. Interfaces* **2018**, *10*, 28232.
- [46] N. Cohen, K. Bhattacharya, *Int. J. Non-Linear Mech.* **2019**, *108*, 81.
- [47] M. Hallaji, A. Seppänen, M. Pour-Ghaz, *Smart Mater. Struct.* **2014**, *23*, 085001.
- [48] T.-C. Hou, K. J. Loh, J. P. Lynch, *Nanotechnology* **2007**, *18*, 315501.
- [49] J.-B. Chossat, H.-S. Shin, Y.-L. Park, V. Duchaine, *J. Mech. Robot.* **2015**, *7*, 021008.
- [50] R. N. Palchesko, L. Zhang, Y. Sun, A. W. Feinberg, *PLOS One* **2012**, *7*, e51499.
- [51] J. D. Eshelby, *Proc. R. Soc. Lond. A* **1957**, *241*, 376.
- [52] S. H. Jeong, K. Hjort, Z. Wu, *Sci. Rep.* **2015**, *5*, 8419.